www.ietdl.org

Published in IET Science, Measurement and Technology
Received on 16th December 2013
Revised on 2nd June 2014
Accepted on 16th June 2014
doi: 10.1049/iet-smt.2013.0279

Special Issue on Green Wireless Internet Technology

ISSN 1751-8822

24-GHz Patch antenna array on cellulose-based materials for green wireless internet applications

Martina Poggiani, Federico Alimenti, Paolo Mezzanotte, Marco Virili, Chiara Mariotti, Giulia Orecchini, Luca Roselli

Department of Engineering, University of Perugia, via G. Duranti 93, 06125 Perugia, Italy
E-mail: federico.alimenti@unipg.it

Abstract: A 24-GHz patch array antenna with integrated feeding network has been fabricated exploiting a multi-layer cellulose-based (i.e. paper) substrate. The adopted microstrip circuitry exploits a copper adhesive laminate that is shaped by a photo-lithographic process and transferred to the hosting substrate using a sacrificial layer. The multi-layer structure is obtained by stacking and gluing two layers of photo-paper with an interposed copper ground plane. The measurements show an input reflection coefficient of about −29 dB at the centre frequency, an operating bandwidth with $S_{11} \leqslant -20$ dB of 540 MHz and a gain of 7.4 dBi. The estimated radiation efficiency is 35%. The proposed design shows the feasibility of low-cost antenna systems for green wireless internet technology and applications up to the boundary between microwaves and millimetre-waves.

1 Introduction

In the near future, internet will fully realise the 4A paradigm, meaning that anyone will have information about anything from anywhere and at anytime. To accomplish this evolution, several key technologies have to converge. First, wireless mobile terminals with very high data-rates must be developed. Considering that the WiFi frequency ranges at 2.4- and 5.8-GHz are full of services and that they are unable to allocate wide-band signals, new, unlicensed microwave and millimetre-waves bands are under consideration. Among several possibilities, both the 24 and the 60 GHz frequencies have recently been proposed by several authors from industry and academia [1–4]. In particular, the 24 GHz Industrial, Scientific and Medical (ISM) frequency band is of wide interest because unlicensed devices and services are permitted and the atmospheric attenuation does not compromise the communication.

Second, a large variety of wireless sensors (i.e. things) will be connected to the network, leading to the so-called Internet-of-Things. These sensors will mostly exploit the Radio Frequency IDentification technology since it is able to provide energy autonomy (i.e. batteryless devices) and (short range) bi-directional communication [5–7]. Third, diffusion of very granular architectures will impose a tremendous cost reduction and, when possible, a circuital simplification. Last but not least, the huge number of mobile terminals, together with the increasing deployment of miniaturised unrecoverable sensors, will result in a potential risk of environmental pollution. As a consequence, eco-compatible (recyclable and biodegradable) materials and green electronic processes shall be adopted [8].

To achieve a high miniaturisation level and to limit the bill-of-material, radio frequency and microwave front-ends should exploit integrated circuits whenever is possible [9] and reconfigurability [10–12]. From this point of view, the best solution is constituted by a system-on-chip (SoC) in nano-scale CMOS technology such as shown in [13, 14]. Although such an approach is very suitable for the digital part of the transceiver and for most of the microwave sections (i.e. the active ones), it yields some limitations when low-loss and passive sub-circuits are considered. In this perspective, one particular issue is constituted by the antenna. The antenna, indeed, is almost always one of the largest building blocks in terms of occupied area. This is because its size is constrained to be within a quarter to a half of wavelength for an acceptable radiation efficiency. From this observation, one can simply infer that microwave antennas cannot be integrated directly on silicon, but must be implemented on a different substrate such as, for example, a flexible or conformal printed circuit board (PCB) [15–17]. Thus, in future wireless terminals and sensors, the mass and the volume of the antenna will be very significant compared with that of the SoC (i.e. sigle-chip) transceiver connected to it. As a consequence, according to the fundamental principle of the green electronic, antennas will be one of the devices with major environmental impact.

Recently, it has been demonstrated that cellulose-based materials (i.e. paper) can be used as a substrate for electronic circuits up to microwave frequencies [18–20]. Cellulose, the most common natural polymer, is eco-compatible, biodegradable, flexible and very cheap, representing one of the most interesting choices for the fabrication of recyclable microwave components and antennas [21].

This work describes the design and the experimental characterisation of a 24-GHz patch antenna array on a cellulose-based substrate. The array is constituted by four

patches excited in-phase and with equal amplitude signals. The feeding network is implemented on a multi-layer substrate with power dividers and feeding lines on top (i.e. antenna) and bottom layers, respectively. A common ground plane is placed between these two layers and a via through is used to connect the antenna to the input port. The layout is fabricated exploiting a copper (Cu) adhesive laminate that is shaped by a photo-lithographic process and transferred to the hosting substrate using a sacrificial layer. Adhesive Cu tapes have been recently proposed and adopted to fabricate flexible microwave circuits [22, 23]. The main differences with respect to cured Ag ink are a superior conductivity and the possibility to solder standard electronic devices on it, the typical resolution being of about 150 μm (line width/gap). On the basis of the authors' knowledge, this is the first 24-GHz antenna array ever implemented in a cellulose-based multi-layered substrate.

This paper is structured as follows. Section 2 will describes the adhesive laminate (also referred to in the past as Cu tape) technology, the design of the radiating element and that of the whole antenna. Section 3 will then focus on the experimental validation and optimisation of the designed array; it also contains a table of comparison with the present state-of-the-art about cellulose-based antennas at several operating frequencies. The conclusions will be finally drawn in Section 4.

2 Design

The circuit is realised on a Mitsubishi Electric photo-paper substrate with an adhesive Cu laminate. The paper thickness is $h = 230$ μm, with a relative permittivity $\varepsilon_r = 2.9$ at 24 GHz and a loss tangent $\tan\delta = 0.08$. The Cu tape (from ADVANCE™) has a thickness $t_m = 35$ μm and a conductivity $\sigma_m = 5.8 \times 10^7$ S/m. In [22], it has been shown that the acrylic adhesive layer affects the microstrip propagation characteristics. Such a layer has a thickness $t_a = 30$ μm, a permittivity $\varepsilon_{r,a} = 1.3$ and a loss tangent negligible with respect to that of the paper substrate. The substrate parameters are quoted in Table 1 under the assumption of uniform permittivity distribution.

The roughness of the Mithsubishi Electric photo-paper (glossy side) has been measured with an atomic force microscope (AFM) and is about 0.05 μm. This value is very small for the considered application and can be safely neglected.

The antenna array is realised exploiting the three metal-layers structure shown in Fig. 1. In this configuration, the top layer is devoted to the radiating elements whereas the bottom layer can be used to build the active circuitry of the microwave front-end. With such an approach, a significant miniaturisation is achieved by re-using the area occupied by the antenna. In the present implementation, the bottom layer is only exploited to build the feeding microstrip line. Between the top and the bottom metal layers there is a common ground plane.

Table 1 Substrate parameters

Parameter	Value	Parameter	Value
ε_r	2.9		
h	230 μm	$\tan\delta$	0.08
t_a	30 μm	$\varepsilon_{r,a}$	1.3
t_m	35 μm	σ_m	5.8×10^7 S/m

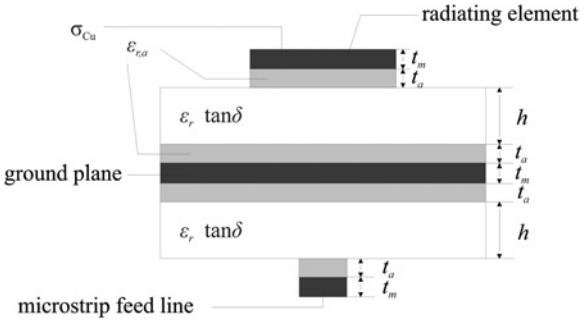

Fig. 1 *Stack-up of the adopted multi-layer substrate exploiting the adhesive Cu-tape*

As it can be seen, a thin adhesive layer remains interposed between metal and substrate
Another Cu tape is used to realise the ground plane

2.1 Single-patch design

The design of the patch array antenna was conceived having two steps: the first one, preparatory to the second, was the design and the experimental characterisation of a single-patch antenna. Then, using the patch as radiating element, the design of the array was finalised.

The feeding line of the patch antenna is realised on the same plane of the radiating element. As a consequence, the substrate is composed of a single sheet of photo-paper and two layers of adhesive Cu laminate, one for antenna implementation (top layer) and one, right below, for the ground plane. Fig. 2 shows the antenna layout. The multi-layer nature of the substrate (paper, adhesive and metal) does not allow analytic synthesis. For this reason,

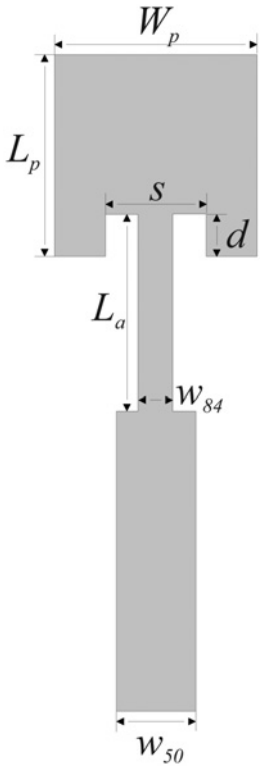

Fig. 2 *Layout of the radiating element (single patch)*

The mechanical dimensions are: $L_p = 3.99$ mm; $W_p = 3.90$ mm; $d = 187$ μm; $s = 686$ μm; $L_a = 2.23$ mm; $W_{84} = 315$ μm and $W_{50} = 789$ μm

the approximate model proposed by Balanis [24] was used as the starting point to perform an initial design.

First, the multi-layer substrate was approximated with a homogeneous substrate of equivalent height (h^{eq}) and equivalent relative permittivity (ϵ_r^{eq}). The relationships for the computation of the equivalent parameters are proposed in [25]. Applying such a model to the substrate shown in Fig. 1 gives

$$h^{eq} = 2t_a + h \tag{1}$$

$$\epsilon_r^{eq} = \frac{h^{eq}}{2(t_a/\epsilon_{r,a}) + (h/\epsilon_r)} \tag{2}$$

In the case of Table 1, the equivalent substrate is characterised by: $h^{eq} = 290$ μm and $\epsilon_r^{eq} = 2.31$.

Then, according to Balanis, the design starts with an initial guess of the patch width W_p as a function of the resonance (i.e. operating) frequency f_0

$$W_p = \frac{c_0}{2f_0}\sqrt{\frac{2}{\epsilon_r^{eq}+1}} \tag{3}$$

Subsequently, the effective permittivity seen by the patch is evaluated

$$\epsilon_{r,eff} = \frac{\epsilon_r^{eq}+1}{2} + \frac{\epsilon_r^{eq}-1}{2}\frac{1}{\sqrt{1+12(h^{eq}/W_p)}} \tag{4}$$

The fringing E-field effect because of the open ends is now accounted for with a small increase ΔL_p of the patch length

$$\frac{\Delta L_p}{h^{eq}} = 0.412\frac{\epsilon_{r,eff}+0.3}{\epsilon_{r,eff}-0.258}\frac{(W_p/h^{eq})+0.264}{(W_p/h^{eq})+0.8} \tag{5}$$

Finally, the patch length can be obtained with

$$L_p = \frac{c_0}{2f_0\sqrt{\epsilon_{r,eff}}} - 2\Delta L_p \tag{6}$$

The design of the radiating element was carried out at $f_0 = 23.5$ GHz. Exploiting the Balanis equations along with the equivalent (i.e. homogeneous in place of multi-layer) substrate model one obtains: $W_p = 4.96$ mm, $\varepsilon_{r,eff} = 2.15$ and $\Delta L_p = 0.3$ mm. As a result, the first guess estimation of the patch length is $L_p = 4.05$ mm.

The above design was refined by using Computer Simulation Technologies (CST) Microwave Suite [26], a three-dimensional (3D) commercial electromagnetic simulator. During the computer aided design (CAD) optimisation, the patch width has been approximately equated to the patch length (i.e. $W_p \simeq L_p$). In particular, the following steps are considered as follows:

- Evaluation of the microstrip characteristic impedance accounting for the multi-layer substrate and sizing (i.e. determination of the line width) of both feeding and input lines.
- Tuning of the patch length L_p so as to set the patch resonance at the operating frequency.
- Design of a quarter-wave impedance transformer with the constraint that the microstrip line is not too narrow for the practical feasibility of the layout. A value of 315 μm was chosen in the presented case, thus setting to $Z_t = 84\ \Omega$ the characteristic impedance of the transformer.
- For a characteristic impedance $Z_0 = 50\ \Omega$ the input patch impedance Z_i should be $Z_i = Z_t^2/Z_0$ which is a quantity about 140 Ω.
- Determination of the inset-feed depth d to have a patch input impedance equal to the computed Z_i.
- Simulation of the whole antenna and fine tuning.

The dimensions of the single patch are quoted in the caption of Fig. 2. It is worth noticing that the obtained length is only 1.5% away from that given by the Balanis equations. Fig. 3 shows the simulated radiation diagrams of the radiating element. These shapes are in agreement with those expected for a single-patch antenna with finite ground-plane. The gain is 2.9 dBi and the half power beam-width is about 64° in the H-plane.

2.2 Array design

The second phase is the design of the 2 × 2 array microstrip patch antenna working at 24 GHz. The structure is realised

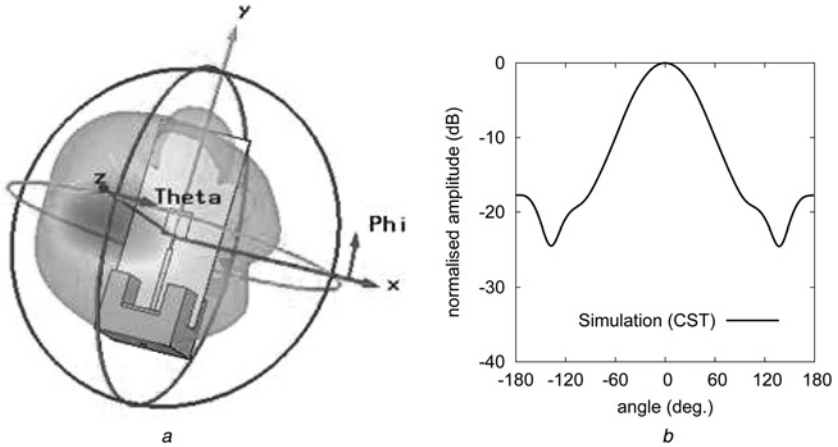

Fig. 3 *Radiation characteristics of the single patch evaluated at the resonance frequency (i.e. 23.6 GHz)*

a 3D pattern
b H-plane cut
The simulations account for both the coaxial to microstrip launcher and the finite size of the ground plane (15 mm in width and 30 mm in length)
The antenna gain is 2.9 dBi, whereas the half power beam-width is about 60° in the H-plane

doi: 10.1049/iet-smt.2013.0279

on the multi-layer substrate described in Fig. 1. To have a broadside radiation, the elements of the array operate in-phase with an uniform distribution of the feeding current. The design procedure can be subdivided in four main phases.

- Optimisation of the single radiating element. First, the patch length was modified in order to tune it to 24 GHz. Second, a new feeding network was conceived. In fact, because of the limited space between the array elements, it is impossible to employ a quarter wavelength impedance transformer for each element.

Finally, loss considerations discourage the use of feeding lines as thin as that at 140 Ω (only 73 μm width). As a consequence the length of the inset-feed has been increased until the input impedance was 100 Ω. This required a small increase of the patch length to compensate for the corresponding frequency shift.

- Array layout determination. The mutual spacing between the elements, in the two directions, is set equal to half wavelength in free-space ($d_x = d_y = 6.2$ mm) in order to avoid the presence of grating lobes. Moreover, an evaluation of mutual coupling among the array elements was performed with the aid of a full-wave analysis.
- Design of the feeding network. The feeding network consists of three power dividers: two simple T-junctions, coplanar to the array and a via through for the connection between the 50 Ω microstrip line (on the bottom layer) and the two quarter wavelength impedance adapters connected to the T-junctions. Fig. 4 shows the layout of the top layer in which are evident the two equivalent T-junctions. Each of them consists of a piece of a 50 Ω microstrip line and two 100 Ω sections (bent of 90°) with a suitable length to reach the radiating elements. Since at the centre of the via through the impedance is 100 Ω, two impedance adapters, to match the 50 Ω of the T-junctions, are introduced.
- Final array configuration. After having characterised the single patch as stand-alone element, specified the array configuration and outlined the feeding network, it remains to optimise the performance of the whole antenna structure. To this purpose one has to: (i) simulate the behaviour of the entire array; (ii) minimise the impact of parasitic effects introduced from the via through by acting on the size of the pads and of the through hole; and (iii) achieve the impedance matching by adjusting the length of the quarter-wave transformers.

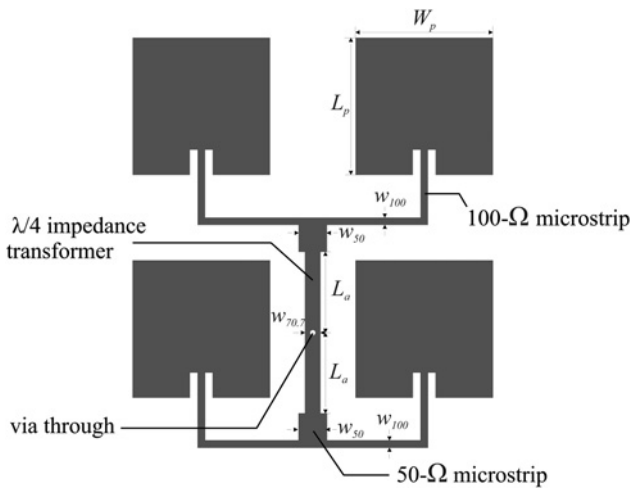

Fig. 4 *Layout of the patch array*

The mechanical dimensions are: $L_p = 3.95$ mm; $W_p = 3.80$ mm; $W_{50} = 785$ μm; $W_{70} = 430$ μm; and $W_{100} = 200$ μm
The spacing between the radiating elements is 6.20 mm in both horizontal and vertical directions
The feeding network excites all the radiating elements in-phase with signal of equal amplitudes
The length of the quarter-wave transformers is $L_a = 2.25$ mm
The whole array is placed inside a square area of only 20 mm side

Fig. 5 shows the radiation pattern of the 2 × 2 patch array. The simulated antenna gain is 6 dBi at 24.15 GHz with an half power beam-width of about 46° in the *H*-plane. It is worth noting that, in the numerical analysis, the ground plane has a finite extension of 20 mm in width and 25 mm in length. This is sufficient to keep the front-to-back gain ratio below −16 dB (i.e. about 40 times in a linear scale). The measured radiation diagram will be shown in the next section.

3 Results

The designed prototypes of both radiating element (i.e. single patch) and antenna array have been fabricated exploiting the adhesive Cu laminate method. This method, fully described in [22], will only be briefly recalled here. The fabrication process is composed of five steps. In the first step, a photo-resist film is deposed on the Cu surface. Then the circuit layout is transferred to the photo-resist exploiting a photo-mask, an UV light source and a developer solution to remove the unimpressed film. In the second step, the Cu is wet etched. Such a step exposes the adhesive layer where the Cu has been removed while, on the opposite side, it remains covered by the protection layer of the original Cu laminate. In the third step, a sacrificial layer is attached on the Cu side and then the protection layer is removed. The sacrificial layer has a very important function to keep the relative distances among the layout features even when these are not physically connected. Such a layer is a piece of saturated flat paper backing tape with natural rubber adhesive [27]. In the fourth step, the etched metal is transferred to the hosting paper substrate and, finally, the sacrificial layer is removed. This last step also removes most of the exposed adhesive material. Such an effect is stronger if a plastic adhesive tape is used as sacrificial layer.

3.1 Single-patch results

To provide an experimental validation of the developed design, first a stand-alone radiating element has been characterised.

Fig. 6 shows the fabricated prototype. The layout in Fig. 2 has been obtained adopting a compensation for the over-etching because of the Cu laminate thickness (35 μm). After the etching and the layer transfer procedure all the mechanical dimensions have been verified with an optical microscope equipped with a calibrated micro-metric scale. The implementation error has been found to be well below 8%, this limit being reached only in the case of the thinner features (i.e. the high-impedance microstrip lines of the feeding network). The measured mechanical dimensions are quoted in the caption of Fig. 2 and have been used for the final electromagnetic simulations of the structure.

Then the single-patch antenna has been contacted with a southwest coaxial to microstrip launcher and measured exploiting a 40 GHz Vector Network Analyzer from

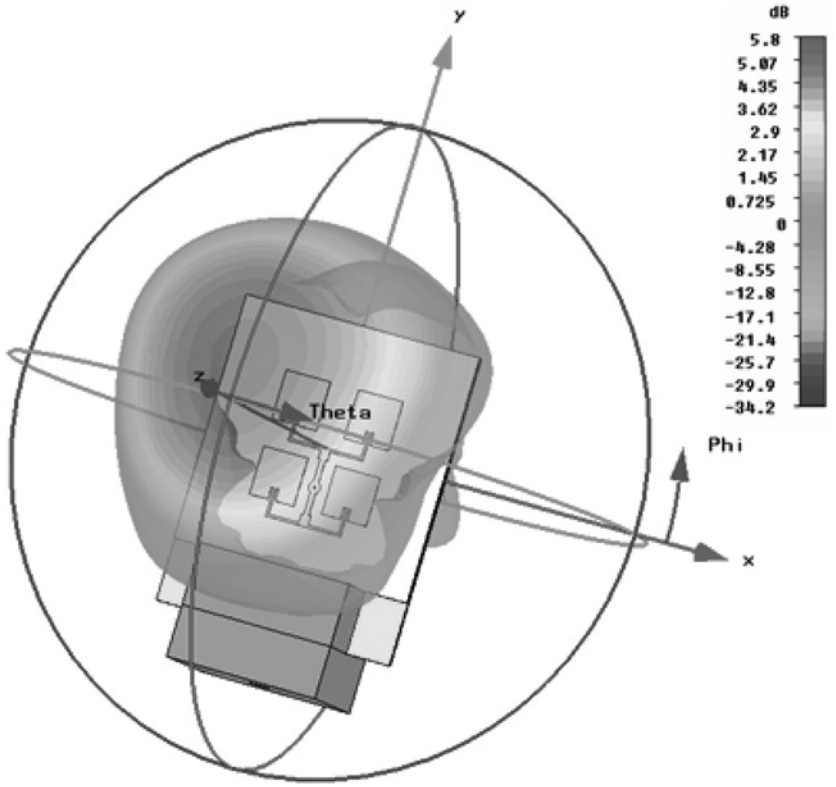

Fig. 5 *Simulated radiating pattern of the patch array (3D view)*

The antenna gain is 6 dBi whereas the whole radiation efficiency (i.e. including the feeding network losses) is about 37%
The simulations account for both the coaxial to microstrip launcher and the finite size of the ground plane (20 mm in width and 25 mm in length)
Note that the slight tilt of the beam along the *E*-plane (about 7°) is because of the microstrip-to-coaxial launcher

Fig. 6 *Photographs of the fabricated radiating element (i.e. single patch) with the coaxial to microstrip launcher used during the measurements*

Agilent (model PNA N52230A). A one-port calibration procedure has also been performed in order to set the reference plane at the input of the launcher. The measured reflection coefficient is shown in Fig. 7 and is in a good agreement with the numerical simulations. In particular the resonance frequency is predicted with a 0.6% error by CST. The simulations also include a model of the coaxial to microstrip launcher used in the measurements.

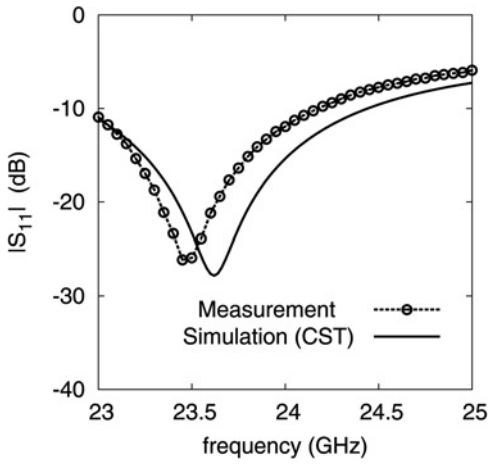

Fig. 7 *Input reflection coefficient of the radiating element (single patch): comparison between EM simulations and measurements*

The simulations also include a model of the coaxial to microstrip launcher used in the measurements

doi: 10.1049/iet-smt.2013.0279

A further experiment (not shown in Fig. 7) was carried out to determine the tuning sensitivity of the radiating element with respect to variation of the patch length. Two patch prototypes with slightly different lengths were compared. It has been discovered that the sensitivity of the resonance frequency with respect to L_p is of about −6 MHz/μm. As it will be shown below, this value can be estimated quite well exploiting the approximate theory of Balanis. The resonance frequency, in fact, is easily obtained by reversing (6)

$$f_0 = \frac{c_0}{2\sqrt{\epsilon_{r,\text{eff}}}\left(L_p + 2\Delta L_p\right)} \tag{7}$$

The tuning sensitivity of the radiating element, T_s, is defined as the derivative of the above expression with respect to L_p

$$T_s = \frac{\partial f_0}{\partial L_p} = -\frac{c_0}{2\sqrt{\epsilon_{r,\text{eff}}}\left(L_p + 2\Delta L_p\right)^2} \tag{8}$$

In the above expression, the patch width W_p has been assumed to be constant and, as a consequence, ΔL_p is not a function of L_p. Using (7) in (8), one obtain

$$T_s = -2\frac{f_0^2}{c_0}\sqrt{\epsilon_{r,\text{eff}}} \tag{9}$$

Observe that, under the Balanis approximations, the tuning sensitivity is a function of the resonance frequency and of the effective dielectric constant only. Computing (9) for $f_0 = 23.5$ GHz and $\varepsilon_{r,\text{eff}} = 2.15$, that is, in the case of the single patch discussed previously, one obtains $T_s = -5.4$ MHz/μm, in good agreement with the measured value. At this point, it is worth noticing that the knowledge of T_s can be used to adjust, even in an experimental way, the resonance frequency of the array (see below).

3.2 Array results

To fabricate the antenna array three adhesive Cu laminates need to be etched, aligned and then stuck together. These three layers are: the top layer with the four patches and the power dividing network, the intermediate layer with the ground plane and the bottom layer with the feeding microstrip line. The ground metal is discharged in a central hole (diameter equal to about 1.05 mm) to allow the signal

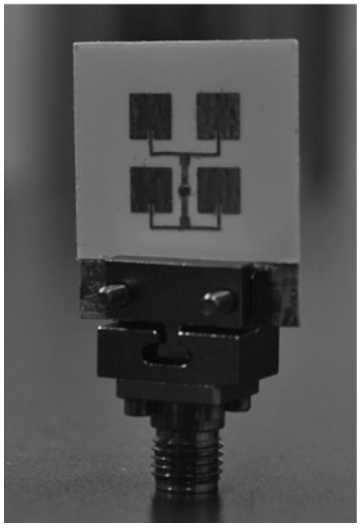

Fig. 8 *Photographs of the fabricated patch array test jig*

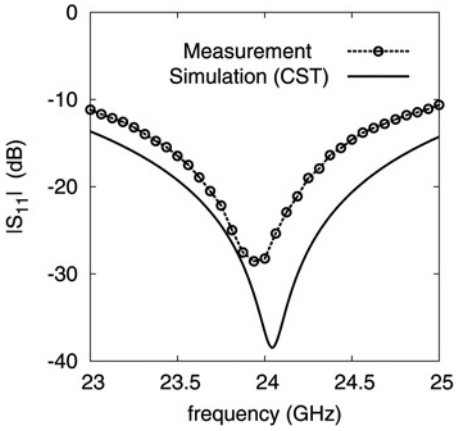

Fig. 9 *Input reflection coefficient of the patch array: comparison between EM simulations and measurements*

The dashed line shows the measurements prior the layout optimisation
The −20 dB antenna bandwidth is of about 540 MHz

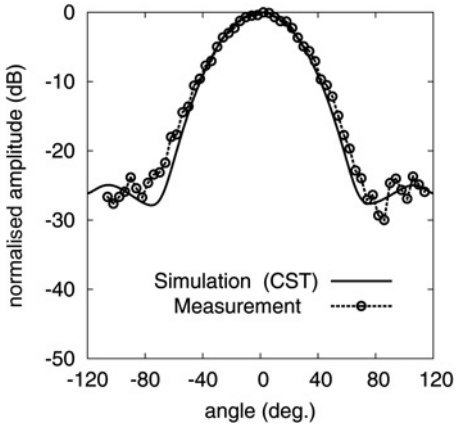

Fig. 10 *Radiation diagram of the 2 × 2 array in the H-plane at 24.15 GHz*

Comparison between measurement and CST simulation
The half power beam-width is equal to about 48°

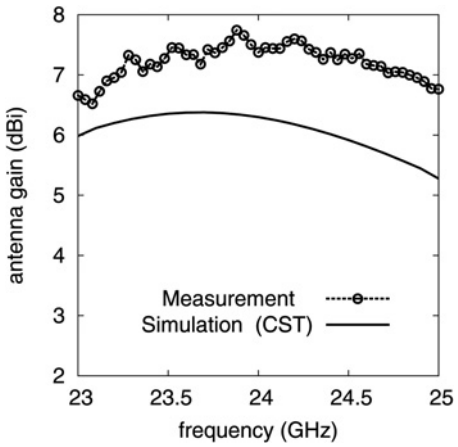

Fig. 11 *Gain of the whole patch array against frequency: comparison between measurement and simulation*

Table 2 State-of-the-art for cellulose-based antennas

Ref.	Type	f_0, GHz	BW, %	Θ, deg.	η, %	Gain, dBi
[28]	inverted F	2.45	24	n.a.	82	1.2
[29]	slotted monopole	5	36	omni	71	2.0
[30]	slot and monopoles	6.5	73	n.a.	75	2.4
[31]	Vivaldi	11	UWB	50	n.a.	6.0
this work	patch array	24	2.3	48	35	7.4

connection between feeding line and antenna. Such a connection is implemented with a via-through in the form of a soldered Cu wire (diameter about 0.19 mm). The final prototype is shown in Fig. 8 and, according to the simulations, has an overall size of 20×25 mm^2.

The feeding line of the antenna has then been contacted with a precision end-launcher connector (from southwest microwave) and then the antenna is characterised with the VNA. The comparison between measured and simulated input reflection coefficient is shown in Fig. 9. The agreement between experiments and numerical model is very good, with a frequency error between the two deep points of about 90 MHz, that is, less than 0.4%.

The radiation characteristics of the array have been determined by means of an anechoic chamber. Fig. 10 shows the comparison between the measured and simulated radiation diagram (*H*-plane cut) at the operating frequency of the array, that is, at 24.15 GHz. The southwest coaxial to microstrip launcher used in the experiment is accounted for in the simulations also. The agreement between measurements and simulations is within ±10%, for the main-lobe, whereas the side-lobe level is well predicted by the simulations. The measured 3 dB beam-widths are $\Theta_e = 55°$ in the *E*-plane cut and $\Theta_h = 48°$ in the *H*-plane cut.

Then, the antenna gain G_a has been determined. To this purpose, the three-antenna method [24, p. 1031] was adopted. In particular, the measurements were corrected for the return loss of each antenna, as required by the IEEE Std. 145-1993. The free-space link was 32 cm long (i.e. beyond the far-field limit for the present antenna) and the free-space loss was measured with a VNA. The obtained results are reported in Fig. 11 against frequency. The graph has a peak at 24 GHz reaching a value equal to 7.4 dBi. Also note that the gain decreases about 1.5 dB between 23 and 25 GHz, indicating that the structure is well centred in the design frequency band. The agreement between experiment and CST simulations is within 1 dB (i.e. about 25% in linear scale), whereas the discrepancies can be attributed to the multi-path reflections. These are because of the fixture used to hold the two antennas in the right position (it was not possible to carry-out the gain measurements in the anechoic chamber).

Finally, according to [24, p. 51] the array directivity D_a can be approximated by

$$D_a \simeq \frac{4\pi(180/\pi)^2}{\Theta_e \Theta_h} \tag{10}$$

where Θ_e and Θ_h are the half power beam-widths (*E*- and *H*-planes, respectively) in degrees. Using the previous measurements for these quantities (i.e. $\Theta_e = 54°$ and $\Theta_h = 48°$) one obtains $D_a \simeq 15.6$ in linear scale or 11.9 dBi. Since the radiation efficiency is, by definition, the ratio between antenna gain and directivity and considering that $G_a = 7.4$ dBi (5.5 in linear scale) one obtain

$$\eta_a = \frac{G_a}{D_a} = \frac{5.5}{15.6} \simeq 0.35 \tag{11}$$

This means that the measurements allow for an estimation of the radiation efficiency close to 35%, in good agreement with 37% predicted by the CST simulator.

Table 2 summarises, to the best authors' knowledge, the state-of-the-art for cellulose-based antennas. As it is apparent from the comparative analysis, the design proposed in this paper is operated at the highest frequency ever reached by a paper substrate microwave antenna. Furthermore, it is one of the very few antenna arrays implemented on green materials. Finally, it exploits a multi-layer technology for space saving.

4 Conclusions

In this work, for the first time, a complete patch 2×2 array antenna has been fabricated and successfully experimented exploiting a multi-layer cellulose (i.e. paper) substrate. The antenna operates at the record frequency of 24 GHz with an input reflection coefficient of about −29 dB, an operating bandwidth with $S_{11} \leq -20$ dB of 540 MHz. The array gain is about 7.4 dBi with an estimated radiation efficiency of 35%. To achieve a significant miniaturisation, the antenna is realised exploiting a multi-layered structure. In this way, the bottom antenna face can be used for the active front-end paper. The whole array has a size of only 20×25 mm^2.

A new fabrication process has also been exploited for the circuit implementation. It is based on a Cu adhesive laminate that is etched by means of a photo-lithographic technology. Then the layout features are transferred to the cellulose-based substrate via a sacrificial layer. The main advantages of the Cu laminate are a very high conductivity (i.e. low-loss) and the possibility to solder standard electronic components on it.

The proposed design shows the feasibility of low-cost antenna systems for green wireless Internet technology and applications up to the boundary between microwaves and millimetre-waves.

5 Acknowledgments

The authors are indebted to Davide Maiarelli, Enrico D'Agostino, Giampiero Sampalmieri and Fabio Tossici of Thales-Alenia Space, Italy, for the anechoic-chamber measurements. The authors are very grateful to Dr. Luca Valentini, University of Perugia, Italy, for the characterization of the substrate roughness by the Atomic-Force Microscope. Agilent Technologies, Computer Simulation Technologies (CST) are finally acknowledged for the donation of the software licenses, which make this research possible.

doi: 10.1049/iet-smt.2013.0279

This work was partially supported by the 'ARTEMOS' and 'ENLIGHT' European projects (ENIAC-JU, call 3 2010) and by the 'GRETA' national project (call 2011).

6 References

1 Wargo, J.: Unlicensed 24 GHz point to point wireless backhaul option, 2010 May. Available at: http://www.aowireless.com

2 (2012, Jun.) Highspeed internet provider selects SAF freemile 24 GHz to extend its network in Hawaii. SAF Tehnika JSC. Available at: http://www.openpr.com/news/226290/

3 Alimenti, F., Mezzanotte, P., Tasselli, G., Battistini, A., Palazzari, V., Roselli, L.: 'Development of low-cost 24-GHz circuits exploiting system-in-package SiP approach and commercial PCB technology', *IEEE Trans. Compon. Packag. Manuf. Technol.*, 2012, **2**, (8), pp. 1265–1274

4 Ercoli, M., Dragomirescu, D., Plana, R.: 'Reduced size high performance transformer balun at 60 GHz in CMOS 65 nm technology', *Microelectron. J.*, 2012, **43**, (11), pp. 737–744

5 Hagerty, J., Helmbrecht, F., McCalpin, W., Zane, R., Popovic, Z.: 'Recycling ambient microwave energy with broad-band rectenna arrays', *IEEE Trans. Microw. Theory Techn.*, 2004, **52**, (3), pp. 1014–1024

6 Kim, S., Georgiadis, A., Collado, A., Tentzeris, M.: 'An inkjet-printed solar-powered wireless beacon on paper for identification and wireless power transmission applications', *IEEE Trans. Microw. Theory Techn.*, 2012, **60**, (12), pp. 4178–4186

7 Alimenti, F., Roselli, L.: 'Theory of zero-power RFID sensors based on harmonic generation and orthogonally polarized antennas', *Progr. Electromagn. Res.*, 2013, **134**, pp. 337–357

8 Orecchini, G., Yang, L., Rida, A., Alimenti, F., Tentzeris, M.M., Roselli, L.: 'Green technologies and RFID: present and future', *Appl. Comput. Electromagn. Soc. J.*, 2010, **25**, (3), pp. 230–238

9 (2010, ENIAC-JU, call3) Agile RF transceivers and front-ends for future smart multi-standard communication applications. ARTEMOS project. Available at: http://www.artemos.eu

10 Elfergani, I., Sadeghpour, T., Abd-Alhameed, R., *et al.*: 'Reconfigurable antenna design for mobile handsets including harmonic radiation measurements', *IET Microw. Antennas Propag.*, 2012, **6**, (9), pp. 990–999

11 Elfergani, I., Hussaini, A., Rodriguez, J., See, C., Abd-Alhameed, R.: 'Wideband tunable PIFA antenna with loaded slot structure for mobile handset and LTE applications', *Radioengineering*, 2014, **23**, (1), pp. 345–355

12 Alimenti, F., Virili, M., Mezzanotte, P., *et al.*: 'A RF-MEMS based tunable matching network for 2.45-GHz discrete-resizing CMOS power amplifiers', *Radioengineering*, 2014, **23**, (1), pp. 328–337

13 Zito, D., Pepe, D., Mincica, M., *et al.*: 'SoC CMOS UWB pulse radar sensor for contactless respiratory rate monitoring', *IEEE Trans. Biomed. Circuits Syst.*, 2011, **5**, (6), pp. 503–510

14 Jatlaoui, M.-M., Dragomirescu, D., Ercoli, M., *et al.*: 'Wireless communicating nodes at 60 GHz integrated on flexible substrate for short-distance instrumentation in aeronautics and space', *Int. J. Microw. Wirel. Technol.*, 2012, **4**, pp. 109–117

15 Dierck, A., Rogier, H., Declercq, F.: 'A wearable active antenna for global positioning system and satellite phone', *IEEE Trans. Antennas Propag.*, 2013, **61**, (2), pp. 532–538

16 Cook, B., Tehrani, B., Cooper, J., Tentzeris, M.: 'Multilayer inkjet printing of millimeter-wave proximity-fed patch arrays on flexible substrates', *IEEE Antennas Wirel. Propag. Lett.*, 2013, **12**, pp. 1351–1354

17 Vanveerdeghem, P., Torre, P.V., Stevens, C., Knockaert, J., Rogier, H.: 'Flexible dual-diversity wearable wireless node integrated on a dual-polarised textile patch antenna', *IET Sci. Meas. Technol.*, 2014, doi: 10.1049/iet-smt.2013.0224

18 Yang, L., Rida, A., Vyas, R., Tentzeris, M.M.: 'RFID tag and RF structures on a paper substrate using inkjet-printing technology', *IEEE Trans. Microw. Theory Techn.*, 2007, **55**, (12), pp. 2894–2901

19 Alimenti, F., Mariotti, C., Mezzanotte, P., Dionigi, M., Virili, M., Roselli, L.: 'A 1.2 V, 0.9 mW UHF VCO based on hairpin resonator in paper substrate and Cu adhesive tape', *IEEE Microw. Wirel. Compon. Lett.*, 2013, **23**, (4), pp. 214–216

20 Alimenti, F., Mezzanotte, P., Giacomucci, S., *et al.*: '24-GHz single-balanced diode mixer exploiting cellulose-based materials', *IEEE Microw. Wirel. Compon. Lett.*, 2013, **23**, (11), pp. 596–598

21 Orecchini, G., Palazzari, V., Rida, A., Alimenti, F., Tentzeris, M.M., Roselli, L.: 'Design and fabrication of ultra-low cost radio frequency identification antennas and tags exploiting paper substrates and inkjet printing technology', *IET Microw. Antennas Propag.*, 2011, **5**, (8), pp. 993–1001

22 Alimenti, F., Mezzanotte, P., Dionigi, M., Virili, M., Roselli, L.: 'Microwave circuits in paper substrates exploiting conductive adhesive tapes', *IEEE Microw. Wirel. Compon. Lett.*, 2012, **22**, (12), pp. 660–662

23 Catarinucci, L., Colella, R., Tarricone, L.: 'Smart prototyping techniques for UHF RFID tags: electromagnetic characterization and comparison with traditional approaches', *Progr. Electromagn. Res.*, 2012, **132**, pp. 91–111

24 Balanis, C.: 'Antenna theory, analysis and design' (John Wiley & Sons Inc., Publications, 2005, 3rd edn.)

25 Alì, W., Al-Charchafchi, S.: 'Using equivalent dielectric constant to simplify the analysis of patch microstrip antenna with multi-layer substrates'. IEEE Int. Symp. of the Antennas and Propagation Society, Atlanta, Georgia, USA, June 1998, pp. 676–679

26 CST – Computer Simulation Technology. Available at: http://www.cst.com

27 Eurocel Msk 121 – High Grade Masking Tape for Automotive Applications. Available at: http://www.eurocel.it

28 Anagnostou, D.E., Gheethan, A., Amert, A.K., Whites, K.W.: 'A direct-write printed antenna on paper-based organic substrate for flexible displays and WLAN applications', *J. Display Technol.*, 2010, **6**, (11), pp. 558–564

29 Abutarboush, H.F., Shamim, A.: 'Paper-based inkjet-printed tri-band u-slot monopole antenna for wireless applications', *IEEE Antennas Wirel. Propag. Lett.*, 2012, **11**, pp. 1234–1237

30 Abutarboush, H., Shamim, A.: 'Conformal and green electronics: a wideband inkjet printed antenna on paper substrate'. Seventh European Conf. on Antennas and Propagation (EuCAP), Gothenburg (SE), April 2013, pp. 3099–3102

31 Cook, B.S., Shamim, A.: 'Inkjet printing of novel wideband and high gain antennas on low-cost paper substrate', *IEEE Trans. Antennas Propag.*, 2012, **60**, (9), pp. 4148–4156